Silicon resonant accelerometer with electronic compensation of input-output cross-talk

V. Ferrari *, A. Ghisla, D. Marioli, A. Taroni

Dipartimento di Elettronica per l'Automazione and INFM, Università di Brescia, Via Branze 38, 25123 Brescia, Italy

Abstract

A resonant accelerometer manufactured in silicon bulk micromachining with electrothermal excitation and piezoresistive detection is presented. The structure is a seismic mass supported by two parallel flexure hinges as a doubly-sustained cantilever, with a resonating microbeam located between the hinges. The acceleration normal to the chip plane induces an axial stress in the microbeam and, in turn, a proportional change in the microbeam resonant frequency. Beam resonant frequency of around 70 kHz and acceleration sensitivity of 35 Hz/g over the range 0–3 kHz were measured on prototypes, in accordance with analytical calculations and simulations. The microbeam operates unsealed at atmospheric pressure, therefore a comparatively low quality factor results due to air damping. In this condition, the effect of the input-output cross-talk was found to be significant. The cross-talk is analyzed and modeled, and an electronic active compensation is proposed. The compensated sensor was inserted into a phase-locked loop oscillator and tested. Reported experimental results show that the sensor performs in excellent agreement with the theoretical predictions.
© 2005 Elsevier B.V. All rights reserved.

Keywords: Accelerometer; Resonant sensor; Cross-talk; Oscillator; MEMS

1. Introduction

In resonant sensors the oscillation frequency at resonance of a mechanical microstructure is changed by a physical or chemical quantity to be measured, in such a way that the value of the measurand quantity can be derived by the shift in the resonant frequency of the microstructure [1–4]. The principle can be applied to several measurands, and resonance parameters other than the frequency, such as amplitude or phase, can also be used in the sensing process. Frequency-output resonant sensors typically offer high sensitivity and stability, potentially leading to good accuracy and resolution. In addition, the "quasi-digital" nature of the frequency signal eases interfacing to readout and processing circuitry and improves noise immunity.

The fabrication of resonant sensors by means of silicon micromachining allows the use of the well-established silicon technology to obtain microdevices with excellent mechanical and elastic properties and a very precise control of the geometry and dimensions of the microstructure [5–7]. Moreover, silicon sensors can be more easily integrated with microelectronic or optical-fibre systems. Several methods for the actuation of the microresonator and detection of the oscillations are reported in the literature [8–13]. For the actuation, the electrostatic, magnetic, piezoelectric, acoustic, electrothermal and optothermal methods can be used. The sensing is typically accomplished by means of piezoresistive, capacitive, optical or piezoelectric methods.

As a particular case of resonant sensors, resonant microaccelerometers have been reported in the literature [14–18] in response to the demand for high-performance all-silicon accelerometers, for instance in the automotive industry. Several examples use the electrothermal excitation and piezoresistive detection, which are straightforward to realize on silicon by means of implanted or deposited resistors [19–20]. As with other operating methods, the electrical nature of the input and output signals allows the

---
* Corresponding author. Tel.: +39 030 3715444; fax: +39 030 380014.
E-mail address: vittorio.ferrari@unibs.it (V. Ferrari).

detection and tracking of the resonant frequency by means of closed-loop circuits that, in this case, feed the amplified signal from the piezoresistors back into the excitation stage of the heater resistor. The whole sensor works as a two-port device with electrical input and output.

An important issue with two-port resonant sensors is that when the acoustic-mechanical path through the resonator has a comparatively high attenuation, i.e. when the quality factor Q is low, any causes of parasitic cross-talk between input and output become increasingly important, because they introduce stray parallel paths that can swamp the resonance behaviour of the sensor.

The electrical cross-talk is discussed in [21,22], and techniques for cross-talk mitigation have been recently reported for microresonators with electrostatic [23,24] and electrothermal [14] actuation.

In this paper, the design, operation and characterization of a micromechanical uniaxial accelerometer are described, based on a resonant microbeam with electrothermal actuation and piezoresistive detection. The microbeam operates unsealed at atmospheric pressure, therefore a comparatively low quality factor results due to air damping. In this condition, the effect of the input-output cross-talk was found to be significant.

The work presents an analysis of the electrical and thermal cross-talk paths between the sensor driving and detection signals, and proposes a purposely designed active electronic compensation circuit.

2. Sensor description and operating principle

The device was fabricated in the SensoNor Normic Multimems bulk micromachining process, offered as a Europractice MPW service for MEMS. A schematic diagram of the accelerometer structure with the relevant dimensions is shown in Fig. 1 (a) and (b).

The structure was realized starting from a (1 0 0) p-type Si substrate and is formed by a doubly-suspended cantilever configuration, where a seismic mass is supported by two parallel flexure hinges which include a central clamped-clamped microbeam. The microbeam has length $l = 600\,\mu m$, width $w = 120\,\mu m$, and thickness $h = 3\,\mu m$ with a rectangular shaped cross section.

The seismic mass with the hinges, and the microbeam are made respectively by an implanted 23-μm thick n-well and a 3-μm thick n-type epitaxial layer, after removal of the bulk p-type Si by anisotropic backside etching with electrochemical etch stop. The suspended structures were released by frontside dry etching through the n-epi layer.

A resistive heater and a piezoresistor are placed at each end of the microbeam, in locations where the excitation and detection efficiency is maximized. Both the heater and the piezoresistor are made by p-doped surface resistors, with nominal sheet resistance of $800\,\Omega$/square.
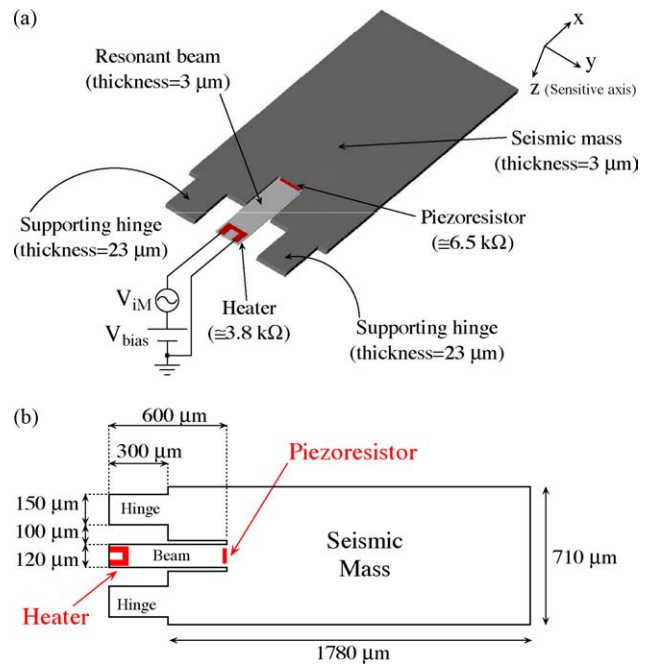

Fig. 1. Schematic view of the sensor structure (a); top view (b).

The microbeam is put into its first flexural resonance by electrothermal actuation via the heater, and the corresponding fundamental frequency is detected by the piezoresistor [25,26,8]. The neutral axes of the supporting hinges and the thinner microbeam are not collinear, so the microbeam undergoes tensile/compressive axial stress induced by the bending of the lateral hinges when the seismic mass oscillates in the positive/negative direction of the z-axis. The microbeam resonant frequency is proportional to the axial stress and, in turn, to the acceleration along z.

A picture of the microsensor is shown in Fig. 2. A top glass protects the chip, which also includes other microstructures irrelevant to this work, though the resonator operates unsealed at ambient pressure.

Flexural vibrations of a clamped-clamped beam, under the hypothesis of high aspect ratio (length/thickness $\gg 1$)
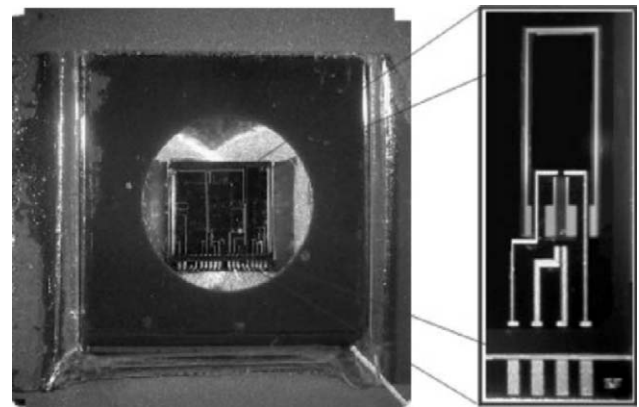

Fig. 2. Picture of the sensor chip with the resonant accelerometer in enlarged view.

and small deflections, can be treated by the theory of Euler–Bernoulli [27–29].

When an axial loading force F is applied to the beam, the resonant frequencies f_n for the various modes can be expressed as [30,31,6]:

$$f_n(F) = \frac{1}{2\pi} \frac{\alpha_n^2}{l^2} \sqrt{\frac{EI}{\rho A}} \sqrt{1 + \gamma_n \frac{Fl^2}{12EI}} \tag{1}$$

where ρ and E are the beam density and Young's modulus, l is the beam length, $A = wh$ is the cross section area, where w and h are the width and thickness, respectively, and $I = wh^3/12$ is the moment of inertia.

In Eq. (1) the beam is assumed narrow enough that any lateral stress is negligible, therefore the Young's modulus E is considered instead of the effective Young's modulus $E/(1 - \nu^2)$, where ν is the Poisson's ratio [32].

The coefficients α_n and γ_n depend on mode number. For the first mode, leading to the fundamental natural frequency f_1, it is $\alpha_1 = 4.730$ and $\gamma_1 = 0.295$ [31].

By inserting into Eq. (1) the dimensions of the microbeam and the material parameters of Si ($E = 1.69 \times 10^{11}$ N/m^2; $\rho = 2.33 \times 10^3$ kg/m^3), the resonant frequency f_1 in the unloaded case, i.e. for $F = 0$, can be calculated, resulting in $f_1 = 72.9$ kHz. The same value within few percents was obtained by finite-element simulations.

To predict the effect on the microbeam frequency f_1 of the acceleration a applied normally to the cantilever surface, the following method was followed. By finite-element simulations the effect of a on the axial force F was determined first. A value of F of 490×10^{-6} N for $a = 100$ g was found. The resultant force F was then inserted into Eq. (1) to calculate the frequency shift for unit acceleration, i.e. the acceleration sensitivity of the microbeam resonant frequency. A sensitivity of 35 Hz/g was obtained. The same result was confirmed by deriving the frequency shift as a function of the applied acceleration entirely by finite-element simulations, without using Eq. (1).

The accelerometer bandwidth is limited to below the first natural frequency of the cantilever, which was calculated to be around 5 kHz. Therefore, a conservative estimation of the accelerometer bandwidth is the 0–3 kHz range.

No stops were inserted into the microstructure to prevent failure due to mechanical overloading, since the adopted dimensions already provide a conservatively high range with a maximum admissible acceleration in excess of 10^4 g.

3. Sensor driving and active cross-talk compensation

To provide excitation to the resistive heater and detect the oscillation induced into the microbeam by the electrothermal actuation, the circuit shown in Fig. 3 was adopted.

The sinusoidal excitation signal $v_i(t) = V_{iM} \sin(\omega t)$ is superimposed on a DC bias V_{bias} and then applied to the heater resistor R_h. The heating power $p(t)$ depends on the square of
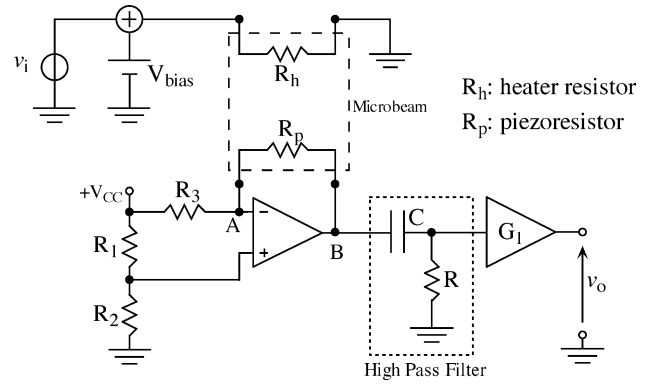

Fig. 3. Sensor excitation–detection circuit.

the total voltage:

$$p(t) = \frac{1}{R_h} \left[V_{bias}^2 + \frac{V_{iM}^2}{2} - \frac{V_{iM}^2}{2} \cos(2\omega t) + 2V_{bias}V_{iM}\sin(\omega t) \right] \tag{2}$$

Therefore, the generated thermal power and, in turn, the induced stress include a static term and two dynamic harmonic components at ω and 2ω.

The detection piezoresistor R_p is connected as the feedback resistor of an operational amplifier forming an active bridge, whose output is AC-coupled by a high-pass filter and further amplified by a factor $G_1 = 1000$. As reported in Fig. 1a), the resistance of the heater and piezoresistor are $R_h = 3.8$ kΩ and $R_p = 6.5$ kΩ, respectively.

The frequency response function between v_i and v_o was measured with a gain-phase analyzer (HP4194A) over the 60–75 kHz range, with $V_{iM} = 2$ V and $V_{bias} = 2.4$ V. Such voltage values result in a static power to the heater of about 2 mW.

The results are shown in Fig. 4, where a peak is visible corresponding to the natural frequency of the beam at 67.1 kHz. The value is in good agreement with the prediction obtained by Eq. (1), though slightly lower. This can be ascribed to the microbeam boundary conditions that are more compliant than in the ideal clamped-clamped case, and to the effect of the temperature rise caused by the driven heater.
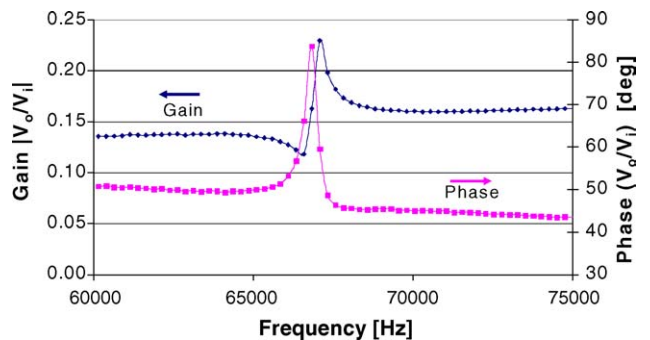

Fig. 4. Sensor frequency response with the excitation–detection circuit around the microbeam resonant frequency.
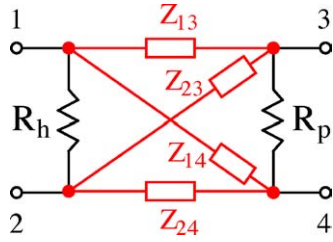
Fig. 5. Model of the electrical cross-talk between heater and piezoresistor.

The resonant–antiresonant behaviour observable in Fig. 4 with a reduced phase shift around the peak is attributed to the stray cross-talk between the heater and the piezoresistor or, more generally, between the sensor input and output.

In resonant sensors, cross-talk phenomena between input and output ports are important [21,22], and they become increasingly influential when the mechanical resonance has a low quality factor. This can have the detrimental effect of preventing the accurate detection and tracking of the resonant frequency, and also limits the operating range.

A major cause of cross-talk is the input-output stray electrical coupling. In a rather general way, the electrical cross-talk, considered as a linear phenomenon, can be represented by a lumped model that includes the coupling impedances Z_{ik}, as shown in Fig. 5.

In the present case, by examining the physical layout of the sensor and the routing of the electrical connections to the bonding pads, it can be assumed that the Z_{ik} are infinite at DC and, at parity of frequency, $Z_{13} \cong Z_{24}$, $Z_{23} \cong Z_{14}$, $|Z_{13}| < |Z_{23}|$ and $|Z_{24}| < |Z_{14}|$.

By considering the connection of the sensor terminals 3 and 4 to the amplifier circuit terminals A and B, two different variants are possible. They are shown in the AC circuit of Fig. 6, where Z_A and Z_B represent the equivalent impedances seen at nodes A and B. From the analysis of the circuits of Fig. 6 and the previous considerations, it is expected that
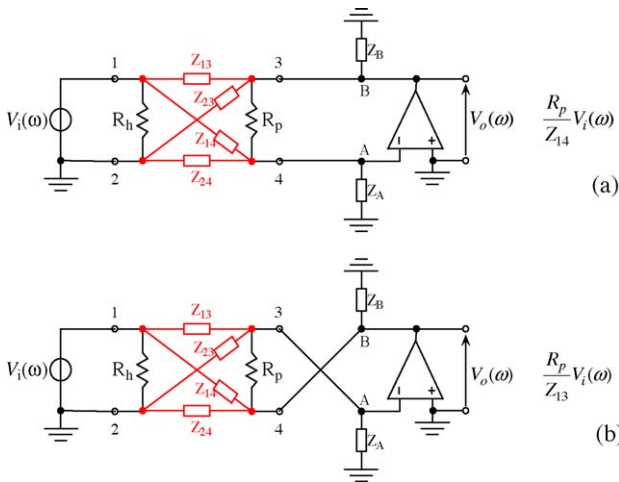

Fig. 6. Possible connections between the sensor outputs 3 and 4 and the circuit inputs A and B.
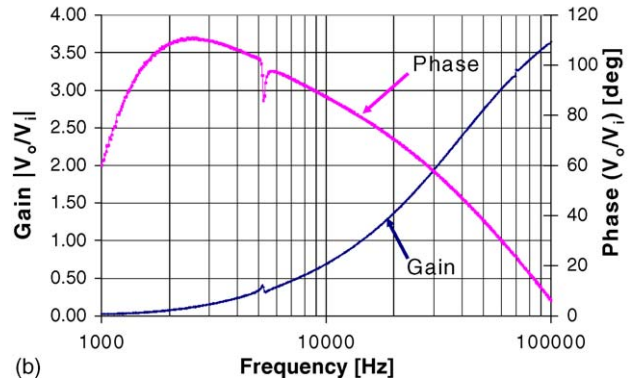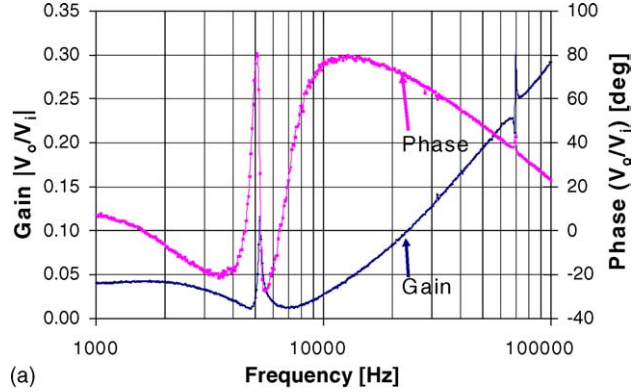

Fig. 7. Measured V_o/V_i frequency response in the two connection variants shown in Fig. 6: (a) case a; (b) case b.

the electrical interference on the output due to the excitation input is smaller in case (a) than in case (b) at any ω.

The frequency response between v_i and v_o was measured in the cases (a) and (b) of Fig. 6. The results are shown in Fig. 7 (a) and (b), respectively. The expectations are confirmed, with a cross-talk significantly higher in case (b) than in case (a). Incidentally, the natural frequency of the cantilever at around 5 kHz can be observed.

An input-output cross-talk due to thermal coupling is also present. From Eq. (2), two different thermal coupling paths can be predicted.

As the first thermal coupling path, the static power $[V_{bias}^2 + (V_{iM}^2/2)]/R_h$, depending on both DC bias and AC amplitude, produces a static temperature distribution along the microbeam, with an average temperature increase ΔT with respect to the temperature of the thermal sink represented by the beam clamps at the seismic mass and substrate.

The temperature increment ΔT causes a static variation in the resistance R_p of the piezoresistor due to both its temperature coefficient and the static stress in the microbeam. Both effects do not reflect on v_o thanks to the AC output coupling.

As an additional effect, the temperature increment ΔT induces a compressive axial force F_T on the microbeam that can be estimated as:
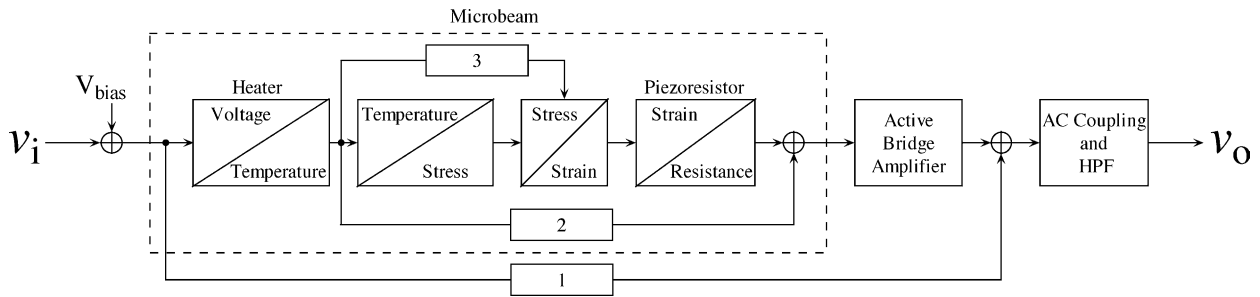
$$F_T = AE\alpha_{th}\Delta T \tag{3}$$

Fig. 8. Block diagram of the microbeam including the cross-talk paths and the excitation–detection circuit.

where $A = wh$ is the beam cross section, E is the Young's modulus, and $\alpha_{th} = 2.5$ ppm/K is the thermal expansion coefficient of silicon. The increment ΔT as a function of the static power can be calculated given the dimensions of the beam and the heater [9], resulting in $\Delta T \cong 1$ K at 2 mW. The value of F_T for $\Delta T = 1$ K calculated from Eq. (3) results around 150×10^{-6} N, which, according to the coefficient of 4.9×10^{-6} N/g derived in Section 2, corresponds to an equivalent acceleration of about 30 g.

This effect, though apparently high enough to obscure the sensor response to acceleration, only produces an initial offset in the sensor resonant frequency, which is negative in sign below the buckling limit [8] and results in an inessential zero error. Provided that the static power $[V_{bias}^2 + (V_{iM}^2/2)]/R_h$ remains constant, such an offset essentially does not vary with the ambient temperature, being the offset related to the overtemperature ΔT of the heated microbeam.

Only in the case that the static power varies due to either V_{iM}, V_{bias}, or both, an effect is produced on the resonant frequency that can be erroneously interpreted as an external acceleration. In this sense, this effect can be considered as a kind of an indirect cross-talk. For example, a 1% change in the static power around the value of 2 mW causes a change in ΔT of 0.01 K, resulting in an equivalent acceleration of 0.3 g. Such a figure can be considered acceptably small with respect to the sensor range.

As the second thermal coupling path, the dynamic power components $[-V_{iM}^2/2 \cos(2\omega t) + 2V_{bias}V_{iM}\sin(\omega t)]/R_h$

produce temperature distributions harmonic at ω and 2ω in the heater area. In principle, such dynamic components could be parasitically reflected at the output via the piezoresistor response. However, thermal waves at frequencies in the order of the resonant frequency are significantly attenuated while propagating along the microbeam, producing a temperature gradient that vanishes at the piezoresistor end. In fact, the penetration depth of a heat wave in silicon is about 20 μm at 70 kHz, and the distance between heater and piezoresistor is 500 μm. Therefore, the dynamic thermal cross-talk is expected to be negligible.

Fig. 8 shows a block diagram that schematically summarizes the different cross-talk contributions discussed. The blocks 1, 2, and 3, respectively represent the electrical cross-talk, the thermal coupling to the piezoresistor with vanishing small AC component and DC component filtered at the output, and the thermal effect on the microbeam expected as a shift in the resonant frequency. From the above considerations it is foreseen that block 1 is influential, block 2 is negligible, and block 3 causes no effect on the resonant frequency of the microbeam as long as the static power to the heater is kept constant.

To actively compensate for the cross-talk, the circuit shown in Fig. 9 was developed. It includes an additional path that can be adjusted in magnitude and phase to counteract the effect of block 1 by injecting the compensating current i_C into the virtual ground of the active-bridge amplifier. In this way, the compensation circuit does not produce any loading
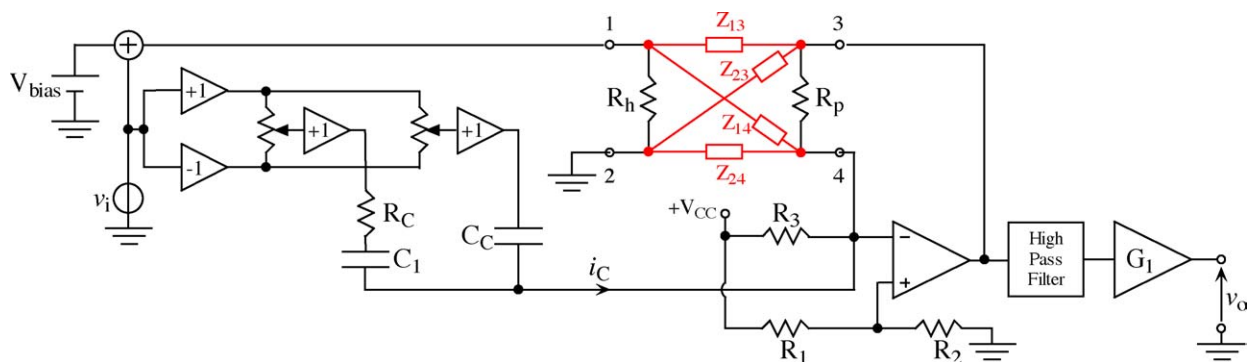

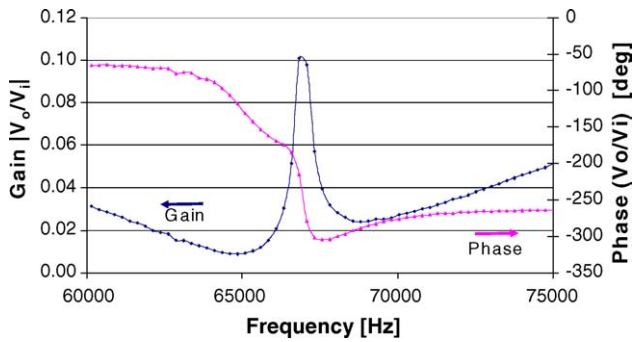Fig. 9. Block diagram of the sensor connected to the excitation–compensation circuit.

Fig. 10. Microbeam frequency response with the cross-talk compensation inserted.

on the active-bridge amplifier, therefore it does not modify the pre-existent cross-talk level but simply cancels its effect at the amplifier output.

The components of i_C in phase and quadrature with v_i are derived by scaling v_i by two independent signed gains and applying the resulting voltages across the compensating
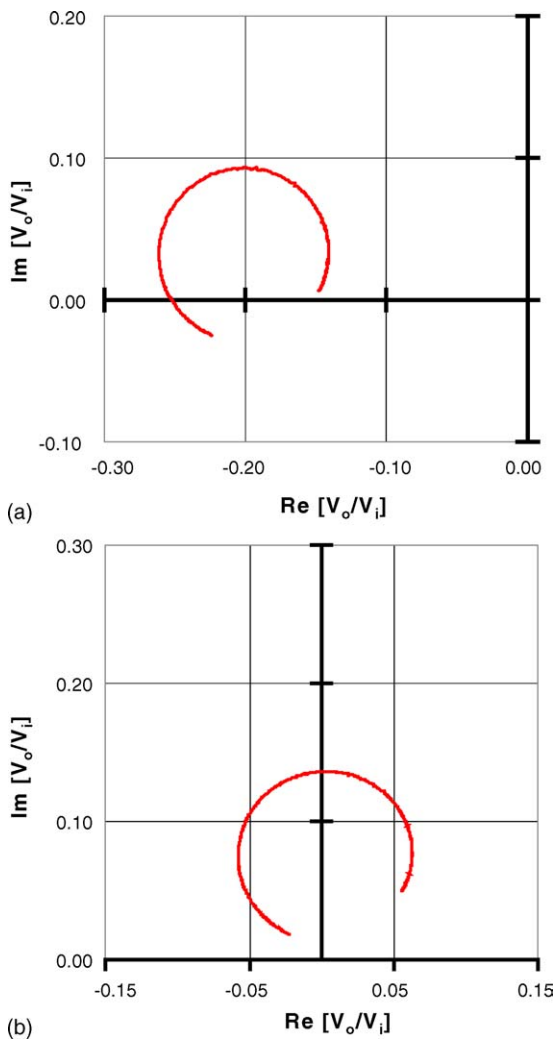

(a)

(b)

Fig. 11. Polar plot of the microbeam frequency response: (a) without cross-talk compensation, (b) with cross-talk compensation.

resistor R_C and capacitor C_C, respectively. The capacitor C_1 only provides DC decoupling, and it is suitably high in value to be negligible at the frequencies of interest.

Fig. 10 shows the results obtained with the compensation circuit. The peak corresponding to the fundamental resonant frequency of the beam can be observed, with a significant improvement over the plot of Fig. 4. A quality factor Q of about 170 results. Such a value is rather low, consistently with the operation of the resonator at atmospheric pressure.

Fig. 11 (a) and (b) show the frequency response in polar representation around the resonant frequency, for both the uncompensated and compensated cases. It can be observed as the compensation appropriately recenters the circle from the offset position due to the cross-talk.

The indirect thermal effect, represented in block 3 of Fig. 8, was tested on a sensor of the same batch actively compensated by the previously described circuit. The measurement results are shown in Fig. 12 (a) and (b), which respectively refer to variations of V_{bias} and of V_{iM}. The predictions are confirmed, with a decrease in the resonant frequency at higher power levels, and a gain enhancement proportional to V_{bias} in agreement with Eq. (2).

The effect caused on the microbeam resonant frequency by variations in the ambient temperature, considered to act uniformly on the whole sensor chip, is responsible for the temperature coefficient of the sensor output frequency. If stress effects induced by thermal expansion mismatches of different materials and packaging are excluded, the
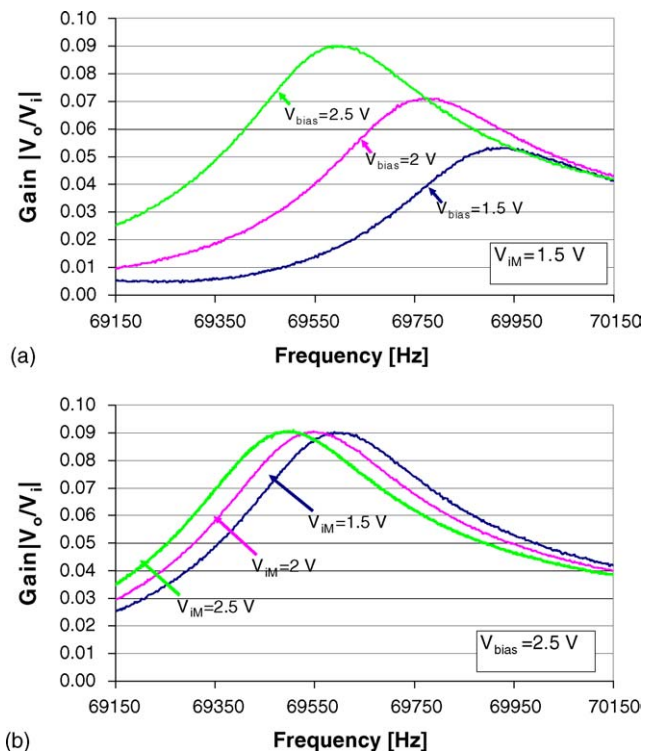

(a)

(b)

Fig. 12. Indirect thermal effect of the static power on the resonant frequency of the microbeam: variations of V_{bias} (a); variations of V_{iM} (b).
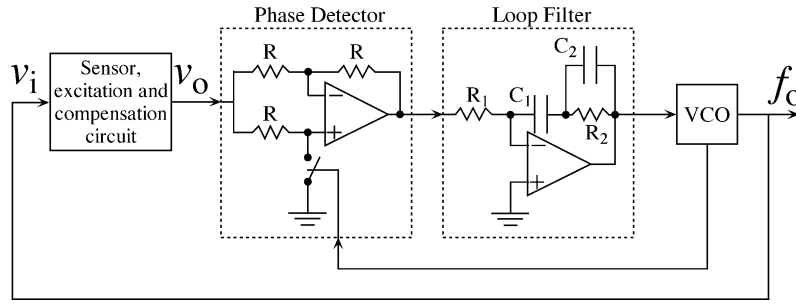
Fig. 13. Phase-locked loop oscillator circuit.

temperature coefficient of the frequency $(\partial f/\partial T)/f$ is determined by the thermal expansion coefficient α_{th} and the temperature coefficient of the Young's modulus $((\partial E/\partial T)/E)$ of silicon [5].

Starting from Eq. (1), under the simplifying assumption that the term due to the axial force F is small enough to be neglected, with $\alpha_{th} = 2.5$ ppm/K and $(\partial E/\partial T)/E = 75$ ppm/K, the frequency temperature coefficient $(\partial f/\partial T)/f$ results in the order of 30 ppm/K. At 70 kHz this reflects into an estimated thermal sensitivity of 2.1 Hz/K, corresponding to an acceleration temperature sensitivity of 0.06 g/K.

4. Electronic oscillator and closed-loop results

The sensor and the excitation–compensation circuit of Fig. 9 were connected in a purposely designed phase-locked loop (PLL) oscillator, as depicted in Fig. 13.

The PLL is formed by a voltage controlled oscillator (VCO) with sinusoidal output (MAX038), a phase detector made by a ± 1 synchronously-switched gain stage, and a loop filter with a pole in the origin and a suitably tailored frequency response to ensure loop bandwidth and stability. The PLL oscillator outputs a sinusoidal signal with a frequency equal to the beam resonant frequency by keeping locked to the condition where the phase between v_i and v_o is equal to $90°$.
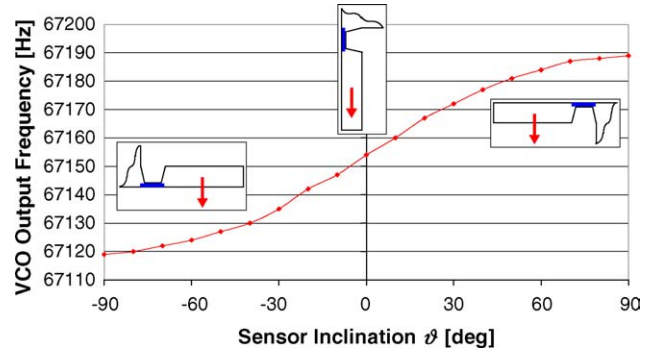

Fig. 14. Oscillator output frequency vs. sensor static inclination (cantilever thickness not to scale in the insert drawings for better clarity).

The sensor connected to the oscillator was mounted on a rotating fixture and subject to variable inclinations between $-90°$ and $90°$, i.e. static accelerations between $-g$ and g.

Fig. 14 shows the measured oscillator frequency f_o versus the inclination angle ϑ, where it can be observed an excellent agreement with the theoretically predicted sensitivity of 35 Hz/g and the expected behaviour proportional to $\sin\vartheta$.

The sensor was then tested under AC acceleration. To this purpose, the circuit of Fig. 13 was modified as shown in Fig. 15. A time-variable acceleration $a(t)$ produces a correspondent variation in the microbeam resonant frequency, i.e.
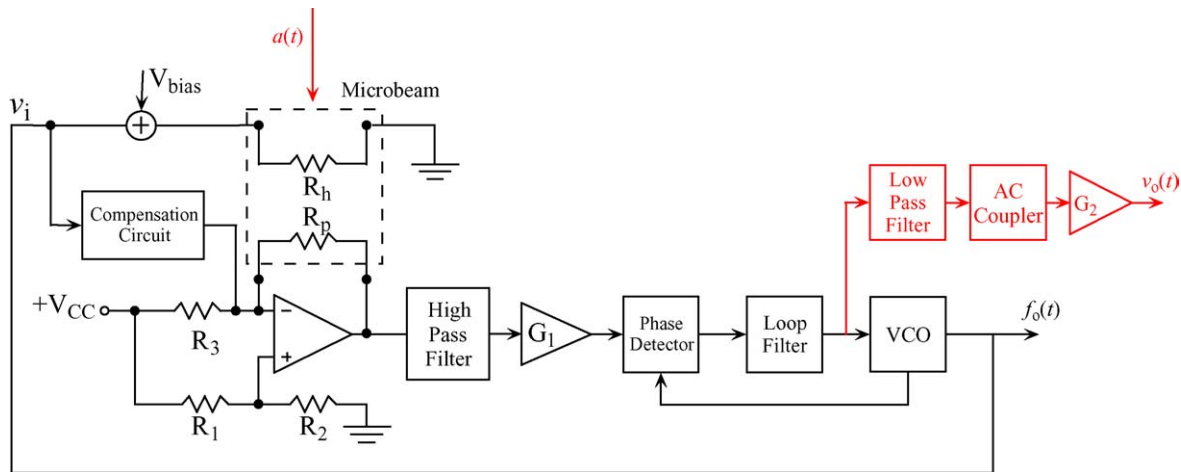

Fig. 15. Block diagram of the *f*-to-*V* demodulator circuit for AC acceleration measurements.
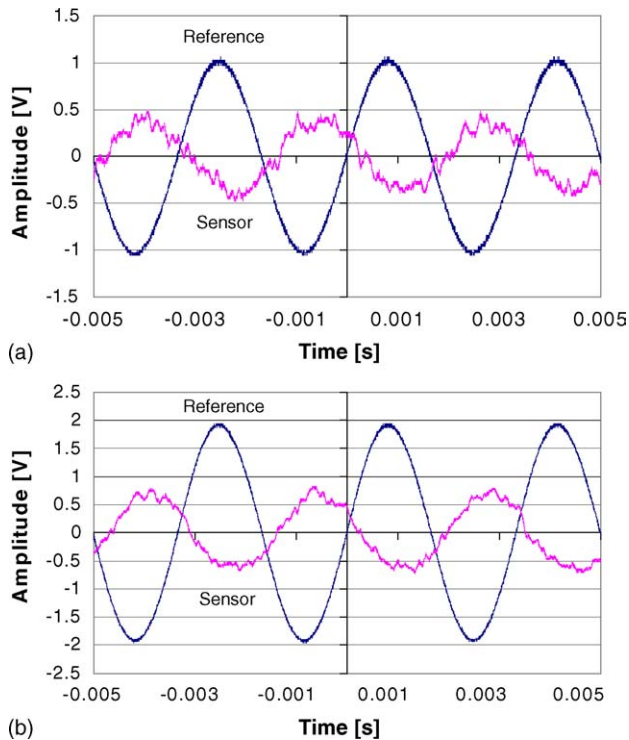
Fig. 16. Comparison between reference accelerometer output and sensor voltage output v_o: applied peak acceleration of 1 g (a), applied peak acceleration of 2 g (b).

a frequency modulation of the carrier f_o tracked by the PLL oscillator. The demodulation is obtained by taking the VCO input voltage suitably amplified out of the loop, so that the resultant output voltage $v_o(t)$ is directly proportional to $f_o(t)$ and, in turn, to the acceleration $a(t)$.

A sinusoidal acceleration $a(t)$ was applied to the sensor by mounting it on a calibration exciter (Brüel & Kjær, 4290) having a built-in reference accelerometer with a sensitivity of 1 V/g. Fig. 16 shows the results obtained at g and 2 g peak amplitudes at 300 Hz. A good reproduction of the sinusoidal acceleration is obtained, with the phase inversion being due to the negative sign of the VCO sensitivity.

5. Conclusions

A silicon bulk-micromachined resonant accelerometer with thermal excitation and piezoresistive detection was realized, analyzed with respect to the input-output cross-talk, and tested. The sensor structure is a seismic mass supported by two parallel flexure hinges, with a resonating microbeam located between the hinges subject to axial stress under an applied acceleration.

The accelerometer has a sensitivity of 35 Hz/g at a frequency of about 70 kHz, corresponding to the first bending mode of the resonant microbeam. The resonator operates unsealed at ambient pressure, causing a quality factor Q as low as 170 that makes it vulnerable to cross-talk effects.

The electrical component of the cross-talk was found to be dominant and, as expected, it could be reduced by adopting a proper readout scheme of the piezoresistor. The thermal component of the cross-talk produces a dynamic effect, which is negligible because the thermal wave at the frequencies in question essentially does not propagate from the heater to the piezoresistor, and a static effect that can be eliminated by AC coupling. The static temperature increment in the heated microbeam, set by the driving level of the heater resistor, influences the resonant frequency by adding a negative offset. This can be considered as a kind of an indirect cross-talk effect, and the control of the heater excitation level is therefore necessary to minimize frequency fluctuations that could be erroneously interpreted as an acceleration signal. A 1% variation in the static power level of 2 mW causes a change in the microbeam average temperature that translates into an equivalent acceleration of 0.3 g.

A circuit for the active compensation of the cross-talk was proposed and successfully verified. The circuit employs an adjustable cancellation of the cross-talk, without introducing any modifications on the pre-existent cross-talk level due to the cancellation circuit itself.

A dedicated phase-locked loop (PLL) oscillator was developed to sustain and track the resonant frequency of the compensated sensor. The accelerometer coupled to the cross-talk compensation circuit and the PLL oscillator was tested under DC and AC accelerations. Despite the poor quality factor of the sensor, the followed approach and the proposed circuits have provided experimental results that are in excellent agreement with the theoretical predictions based on the purely-mechanical analysis of the sensor.

References

[1] P. Hauptmann, Resonant sensors and applications, Sens. Actuators A 25–27 (1991) 371–377.
[2] R.A. Buser, in: H.H. Bau, N.F. de Rooij, B. Kloeck (Eds.), Resonant Sensors in Sensors: Mechanical Sensors, 7, VCH, Weinheim, 1994, pp. 208–279.
[3] R.T. Howe, Resonant Microsensors, Proc. of the 4th International Conference on Solid-State Sensors and Actuators (Tranducers '87), Tokyo, Japan, 2–5 june, 1987, pp. 843–848.
[4] M. Esashi, "Resonant sensors by silicon micromachining", Proc. IEEE Int. Frequency Control Symp., 1996, pp. 609–614.
[5] R.A. Buser, N.F. de Rooij, Resonant silicon structures, Sens. Actuators 17 (1989) 145–154.

[6] M. Esashi, S. Sugiyama, K. Ikeda, Y. Wang, H. Miyashita, Vacuum-sealed silicon micromachined pressure sensors, Proc. IEEE 86 (8) (1998) 1627–1639.

[7] G.T.A. Kovacs, Micromachined Transducers Sourcebook, WCB/McGraw-Hill, New York, 1998.

[8] S. Bouwstra, R. Legtenberg, H.A.C. Tilmans, M. Elwenspoek, Resonating microbridge mass flow sensor, Sens. Actuators A 21–23 (1990) 332–335.

[9] T.S.J. Lammerink, M. Elwenspoek, R.H. Van Ouwerkerk, S. Bouwstra, J.H.J. Fluitman, Performance of thermally excited resonators, Sens. Actuators A 21–23 (1990) 352–356.

[10] L.M. Zhang, D. Walsh, D. Uttamchandani, B. Culshaw, Effect of optical power on the resonance frequency of optically powered silicon microresonators, Sens. Actuators A 29 (1991) 73–78.

[11] J.J. Yao, N.C. MacDonald, A micromachined single-crystal silicon, tunable resonator, J. Microelectromech. Syst. 5 (1995) 257–264.

[12] K. Ikeda, H. Kuwayama, T. Kobayashi, T. Watanabe, T. Nishikawa, T. Yoshida, K. Harada, Silicon pressure sensors integrates resonant strain-gauge on diaphragm, Sens. Actuators A 21–23 (1990) 146–150.

[13] F.R. Blom, D.J. Yntema, F.C.M. van de Pol, M. Elwenspoek, J.H.J. Fluitman, T.J.A. Popma, Thin film ZnO as a micromechanical actuator at low frequencies, Sens. Actuators A 21–23 (1990) 226–228.

[14] M. Aikele, K. Bauer, W. Ficker, F. Neubauer, U. Prechtel, J. Schalk, H. Seidel, Resonant accelerometer with self-test, Sens. Actuators A 92 (2001) 161–167.

[15] D.W. Burns, R.D. Horning, W.R. Herb, J.D. Zook, Sealed-cavity resonant microbeam accelerometer, Sens. Actuators A 53 (1996) 249–255.

[16] C. Burrer, J. Esteve, A novel resonant silicon accelerometer in bulk micromachining technology, Sens. Actuators A 46–47 (1995) 185–189.

[17] C. Burrer, J. Esteve, High-precision BESOI-based resonant accelerometer, Sens. Actuators A 50 (1995) 7–12.

[18] P. Ohlckers, R. Holm, H. Jakobsen, T. Kvisteroy, G. Kittilsland, A. Larsen, M. Nese, S.M. Nilsen, A. Ferber, An integrated resonant accelerometer microsystem for automotive applications, Sens. Actuators A 66 (1998) 99–104.

[19] C. Burrer, J. Esteve, E. Lora-Tamayo, Resonant silicon accelerometers in bulk micromachining technology – An approach, J. Microelectromech. Syst. 5 (2) (1996) 122–130.

[20] D.W. Satchell, J.C. Greenwood, A thermally-excited silicon accelerometer, Sens. Actuators A 17 (1989) 241–245.

[21] C.J. van Mullem, H.A.C. Tilmans, A.J. Mouthaan, J.H.J. Fluitman, Electrical cross talk in two ports resonators, Sens. Actuators A 31 (1992) 168–173.

[22] K. Funk, T. Fabula, G. Flik, F. Larmer, Piezoelectrically driven resonant force sensor: fabrication and crosstalk, J. Micromech. Microeng. 5 (1995) 143–146.

[23] P. Bruschi, A. Nannini, F. Pieri, Electrical measurements of the quality factor of microresonators and its dependence on the pressure, Sens. Actuators A 114 (2004) 21–29.

[24] L. He, Y.P. Xu, Circuit technique to enhance bias stability of silicon resonant accelerometer hybrid-packaged under moderate vacuum, Proc. of the Eurosensors XVIII Conference, Roma, Italy, 13–15 September, 2004.

[25] M.B. Othman, A. Brunnschweiler, Electrothermally excited silicon beam mechanical resonators, Electron. Lett. 23 (14) (1987) 728–730.

[26] C. Burrer, J. Esteve, Thermally driven micromechanical bridge resonators, Sens. Actuators A 41–42 (1994) 680–684.

[27] P.M. Morse, Vibration and Sound, America Institute of Physics, 1981.

[28] W.T. Thomson, Vibration Theory and Applications, George Allen & Unwin Ltd., London, 1966.

[29] P.L. Gatti, V. Ferrari, Applied Structural and Mechanical Vibrations: Theory, Methods and Measuring Instrumentation, E&FN SPON-Taylor & Francis Group, London, 1999.

[30] C.J. van Mullem, F.R. Blom, J.H.J. Fluitman, M. Elwenspoek, Piezoelectrically driven silicon beam force sensor, Sens. Actuators A 25–27 (1991) 379–383.

[31] H.A.C. Tilmans, M. Elwenspoek, J.H.J. Fluitman, Micro resonant force gauges, Sens. Actuators A 30 (1992) 35–53.

[32] R.P. van Kampen, R.F. Wolffenbuttel, Modeling the mechanical behavior of bulk-micromachined silicon accelerometers, Sens. Actuators A 64 (1998) 137–150.

Biographies

Vittorio Ferrari was born in Milan, Italy, in 1962. In 1988 he obtained the Laurea degree in Physics cum laude at the University of Milan. In 1993 he received the Research Doctorate degree in Electronic Instrumentation at the University of Brescia. He is currently an Associate Professor of Electrical and Electronic Measurements at the Faculty of Engineering of the University of Brescia. His research activity is in the field of electronic measuring instrumentation and deals with the design of sensors and the related signal conditioning electronics. Particular topics of interest are acoustic-wave piezoelectric sensors, microresonant sensors and MEMS, oscillators for resonant sensors and frequency-output interface circuits. He is involved in national and international research programmes, and in projects in cooperation with industries.

Alessio Ghisla was born in Brescia, Italy in 1972. In 2001, he received the laurea degree in electronic engineering from the Faculty of Engineering, University of Brescia, Brescia, Italy. From September 2001 to October 2002 he has been collaborating with the Department of Electronics and Automation, University of Brescia. Since November 2002 he has been a PhD student in "Electronic Instrumentation" at the University of Brescia, Brescia. His main research interests are the design and characterization of sensors and of electronic circuit interfaces for sensors, with particular regard to capacitive sensors for position measurement and MEMS sensors.

Daniele Marioli was born in Brescia, Italy, in 1946. He obtained the Electrical Engineering degree in 1969. From 1984 to 1989 he was an Associate Professor in Applied Electronics and since 1989 he has been a Full Professor of Electric and Electronic Measurements at the University of Brescia. His main field of activity is the design and experimentation of analog electronic circuits for the processing of electrical signals from transducers, with particular regard to S/N ratio optimization.

Andrea Taroni was born in 1942. He received the degree in Physical Science from the University of Bologna, Italy, in 1966. He was an Associate Professor at the University of Modena from 1971 to 1986. Since 1986 he has been Full Professor of Electrical Measurements at the University of Brescia. He has done extensive research in the field of sensors for physical quantities and electronic instrumentation, both developing original devices and practical applications. He is author of more than 100 scientific papers.